CrystEngComm

Accepted Manuscript

ROYAL SOCIETY OF CHEMISTRY

www.rsc.org/crystengcomm

Cite this: DOI: 10.1039/c0xx00000x

www.rsc.org/xxxxxx

ARTICLE TYPE

Facile synthesis of porous $MnCo_2O_{4.5}$ hierarchical architectures for high-rate supercapacitors

Wenyao Li,[ab] Kaibing Xu,[a] Guosheng Song,[a] Xiying Zhou,[b] Rujia Zou,[a]* Jianmao Yang,[a] Zhigang Chen,[a] and Junqing Hu[a]*

Received (in XXX, XXX) Xth XXXXXXXXX 200X, Accepted Xth XXXXXXXXX 200X
DOI: 10.1039/b000000x

Porous urchin-like $MnCo_2O_{4.5}$ hierarchical architectures (~ 4-6 μm in diameter) were synthesized by a facile hydrothermal route followed a calcination process, which exhibited a specific capacitance of 151.2 F g^{-1} at 5 mV s^{-1}, outstanding rate capability with 83.6% retention even with the current density increasing to 50 times and excellent long-term cycle stability at progressively varied current densities, which could be considered as a perspective mixed transition metal oxides material for high-rate supercapacitors in some special applications that is not need much high capacitance.

1. Introduction

As novel energy storage devices developed from Leyden Jar invented in 1745, supercapacitors have been paid less attention than batteries until recent years because of a further understanding of the mechanism of their excellent specific capacitances, higher power density, faster charge/discharge process and longer lifespan, which make them attractive as power resources in high power electric devices and electric vehicles[1-3]. According to the mechanism of charge storage, supercapacitors can be classified as two kinds: electrical double layer capacitors (EDLCs) and pseudocapacitors (PCs). Up to now, for PCs, there has been extensive interest in developing commercial attractive transition metal oxides electrodes for their higher specific capacitance than conventional EDLCs due to their fast and reversible redox reaction[4], such as MnO_2,[5] Co_3O_4,[6] NiO,[7] VOx,[8] and etc. However, current research mainly focuses on these simple binary metal oxide materials, and the fast fading of capacitance is still a common drawback in various nanostructured electrode materials.

Mixed transition metal oxides (MTMOs), typically ternary metal oxides with two different metal cations have received an upsurge of interest in recent years due to their promising roles in many energy-related applications.[9-11] The coupling of two metal species could render the MTMOs with rich redox reactions which are beneficial to electrochemical applications. Besides, the various combinations of the cations and the tunable stoichiometric/non-stoichiometric compositions in the MTMOs provide vast opportunities to manipulate the physical/chemical properties. For instance, the ternary metal oxides $NiCo_2O_4$, $CoFe_2O_4$ and $NiMn_2O_4$ have been investigated as high performance electrode materials for supercapacitors.[12-15] Therefore, mixed transition metal oxides with composition other than $NiCo_2O_4$ etc. are also anticipated with great potential for supercapacitors, but such reports are scarce.

In addition to the desirable composition, the performance of MTMOs in power applications also highly depends on the micro-/nanostructures of the materials. In particular, hierarchical structures, which are uniform assemblies of nanoscale primary building blocks (such as nanowires, nanorods, nanosheets and nanoparticles), have drawn special interest due to their exceptional properties and remarkable potential in many fields.[16-18] It is anticipated that such hierarchical structures can well inherit the advantages from the nanoscale building blocks, while the secondary architectures, typically in micro-/nanometer dimension, would bring additional benefits, such as improved stability, uniform porosity and resistance to aggregation, which are the key parameters to influence the electrochemical performances. Although hierarchical structures have been synthesized from many metal oxides,[6,19-22] the controllable synthesis of MTMOs with desirable composition and hierarchical structure still remains a great challenge.

Herein, we have reported a facile synthesis of large scale porous $MnCo_2O_{4.5}$ hierarchical architectures with an urchin-like structure for the first time. It was found that the unique $MnCo_2O_{4.5}$ as a supercapacitor electrode exhibited a specific capacitance of 151.2 F g^{-1} at scan rate of 5 mV s^{-1}. More importantly, this electrode demonstrated an outstanding rate capability with 83.6% retention even with the current density increasing to 50 times, and an excellent long-term cycle stability at progressively varied current densities, which could be considered as a perspective MTMOs for high-rate supercapacitors in some special applications that is not need much high capacitance. The excellent electrochemical performances are mainly attributed to the unique porous and robust hierarchical architectures.

2. Experimental Section

2.1 Preparation

All the reagents used in the experiments were analytical grade (purchased from Sinopharm) and used without further purification. In a typical synthesis, 0.291 g of Cobalt(II) nitrate hexahydrate ($Co(NO_3)_2$•$6H_2O$), 0.126 g of Manganese(II) nitrate

tetrahydrate ($Mn(NO_3)_2$•$4H_2O$) and 0.36 g of urea were dissolved in 40 mL of mixed solution with ethanol and H_2O (V : V = 1 : 1) at room temperature with magnetic stirring to form a clear pink solution and transferred into a 50 mL Teflon lined stainless steel autoclave. The Teflon lined autoclave was sealed and maintained at 90 ºC for 8 h and then naturally cooled down to room temperature. The precipitates were collected by filtration, washed several times with distilled water and absolute ethanol, successively, and then dried at 60 °C for 8 h. Finally, the dry precipitates were calcined at 600 °C for 5 h with a ramping rate of 1°C min^{-1}.

2.2 Material Characterizations

As-prepared products were characterized with D/max-2550 PC X-ray diffractometer (XRD; Rigaku, Cu-Kα radiation), scanning electron microscope (SEM; S-4800), transmission electron microscope (TEM; JEM-2100F) equipped with an energy dispersive X-ray spectrometer (EDS), Thermogravimetric analysis (TGA) and BET (Micromeritics ASAP 2020 surface area analyzer; the samples were outgassed at 100 °C for 6 h under vacuum before measurements were recorded.). The mass of electrode materials was weighed on an XS analytical balance (Mettler Toledo; δ = 0.01 mg).

2.3 Electrochemical Characterizations

Electrochemical performances of the as-obtained products were performed on an Autolab (PGSTAT302N potentiostat) using a three-electrode mode in 1 M KOH solution. Working electrodes were prepared by mixing the as-synthesized $MnCo_2O_{4.5}$ products (80 wt%) with acetylene black (15 wt%), and poly (tetrafluoroethylene) (5 wt%). A small amount of N-methylpyrrolidinone was then added to the mixture. The mixture was then dropped onto graphite paper and dried at 80 ºC overnight to remove the solvent. The reference electrode and counter electrode were saturated calomel electrode (SCE) and platinum (Pt), respectively. The specific capacitance [F g^{-1}] and current density [A g^{-1}] were calculated based on the mass of active materials.

3. Results and Discussion

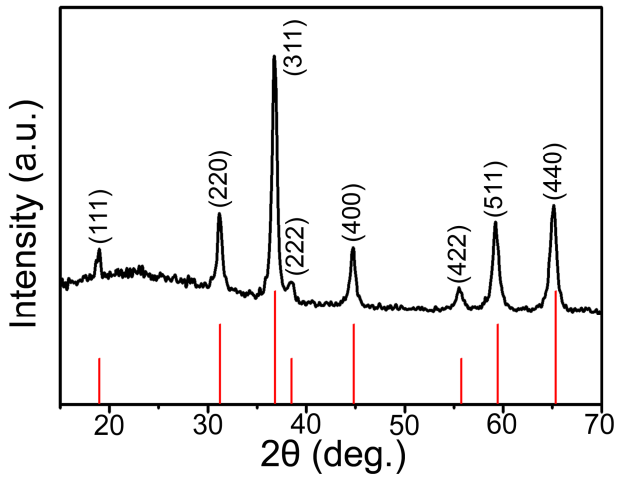

Fig. 1 XRD pattern of the as-obtained $MnCo_2O_{4.5}$ microstructures

Fig. 1 shows the XRD pattern of the obtained product. All of the reflections are consistent with the patterns reported for cubic phase of $MnCo_2O_{4.5}$ (JCPDS card No. 32-0297). No characteristic peaks from precursor impurities such as $Co(NO_3)_2$ and $Mn(NO_3)_2$ are detected. The sharp and narrow diffraction peaks indicate that the $MnCo_2O_{4.5}$ have a high crystallinity. The XRD patterns of the precursor before and after calcination in different temperatures are shown in Fig. S1 (in ESI†).

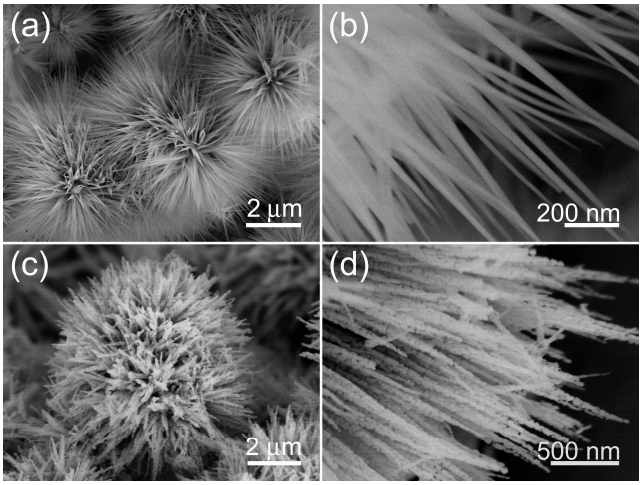

Fig. 2 (a, b) Low and high magnification SEM images of the precursor. (c, d) Low and high magnification SEM images of the urchin-like $MnCo_2O_{4.5}$ hierarchical architectures after calcination.

The low-magnification SEM image of the precursor of $MnCo_2O_{4.5}$ in Fig. 2a reveals the uniform urchin-like hierarchical structures with an average mean diameter of ~ 4-6 μm (a large-scale of as-prepared precursors are showed in Fig. S2, in ESI†). In fact, each urchin-like hierarchical ensemble is composed of many nanoneedles with a diameter of 10 ~ 50 nm from tip to root, Fig. 2b. The low-magnification SEM image of Fig. 2c shows that the $MnCo_2O_{4.5}$ inherited the urchin-like hierarchical structures perfectly after calcination, indicating the robustness of the structures. Meanwhile, the surface becomes coarse and porous, suggesting a highly porous texture shown in Fig. 2d (BET surface specific area value of 22.4 m^2 g^{-1}, Fig. S3, in ESI†). As can be seen, the architectures are composed of 1D nanochains which grew radically to form urchin-like structures from their centers. The nanochains were produced from the oxidation and decomposition of the nanoneedles of the precursor (Fig. S4, in ESI†), which induced the formation of the granular structures. It is well known that porous structure plays a critical role in electrochemical process due to their capability to facilitate mass diffusion/transport (e.g., electrolyte penetration and ions transport) and ensure high electroactive accessible area. Therefore, the porous texture of urchin-like $MnCo_2O_{4.5}$ hierarchical architectures is likely to affect their performance in electrochemical applications.

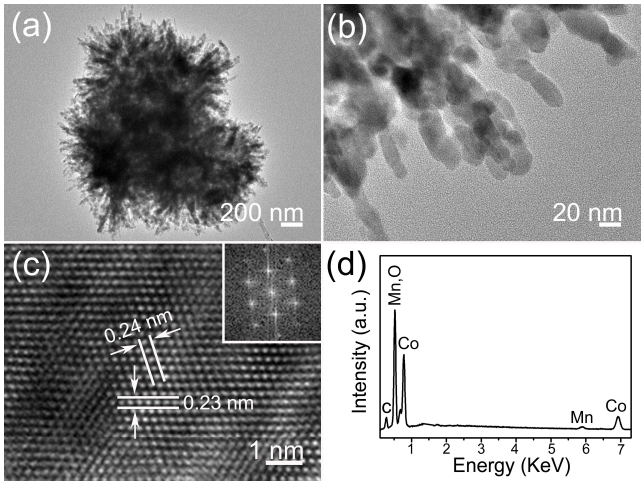

Fig. 3 (a, b) TEM images of the urchin-like $MnCo_2O_{4.5}$ hierarchical architectures. (c) HRTEM image of a nanochain from (b), the inset shows corresponding FFT diffraction pattern. (d) EDX pattern taken from such nanochains.

The TEM image of the $MnCo_2O_{4.5}$ in Fig. 3a shows the whole view of the urchin-like hierarchical structure. The enlarged TEM image shown in Fig. 3b further confirms that the unique structure was composed of 1D nanochains consisting of nanoparticles with a diameter ranging from 10-30 nm, and the nanoparticles were fused together to form the 1D nanochains. The crystal structure of the materials was further characterized by the HRTEM, Fig. 3c. The d-spacings of approximately 0.23 and 0.24 nm correspond to the (222) and (311) planes of the $MnCo_2O_{4.5}$, respectively, which agrees well with the obtained XRD pattern results. To further investigate the detailed structure, the corresponding FFT (the inset in Fig. 3c) was taken from this HRTEM image in Fig. 3c, which indicates the crystal nature. Shown in Fig. 3d is an EDX spectrum recorded from the nanochains, the presences of Mn, Co and O elements are agreement with our synthetic products, and C signal is come from the TEM grid.

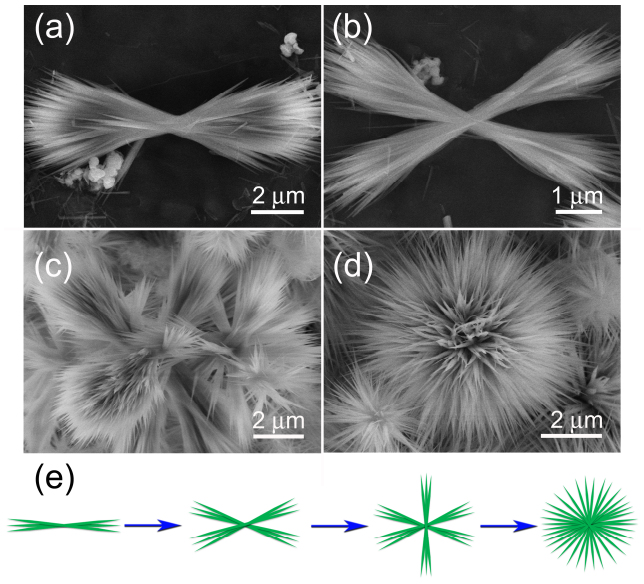

Fig. 4 SEM images of the precursor of $MnCo_2O_{4.5}$ hierarchical structures at different reaction times: (a) 0.5 h, (b) 2 h, (c) 4 h, and (d) 8 h. (e) Proposed mechanism for the growth of the $MnCo_2O_{4.5}$ hierarchical structure

To better understand the formation mechanism of the urchin-like nanostructures, the time-dependent experiments of the hydrothermal process had been carried out. When the reaction time was only 0.5 h, some besom-like nanorod bundles with two ends were obtained as shown in Fig. 4a. With the hydrothermal reaction time increasing to 2 h, there were some secondary branches growing from the middle part of the primary nanorod, indicating a bifurcation phenomenon happens under the current conditions, and the morphology of branches was similar to the products in 0.5 h, as shown in Fig. 4b. Further increasing the reaction time to 4 h, Fig. 4c, some crossed-linked besom-like nanorod bundles would be formed, with much smaller nanorods growing from the two ends of the besom-like nanorod bundles. Interestingly, with continuous increasing the reaction time, the bifurcation phenomenon gradually enhanced and the besom-like nanorods continuously evolved and formed into urchin-like spheres under 8 h reaction time finally, as shown in Fig. 4d. Based on the above results, the whole process can be expressed as depicted in Fig. 4e. This formation process seems to be a common phenomenon in crystal growth process, and also can be observed in several material systems.[23-25]

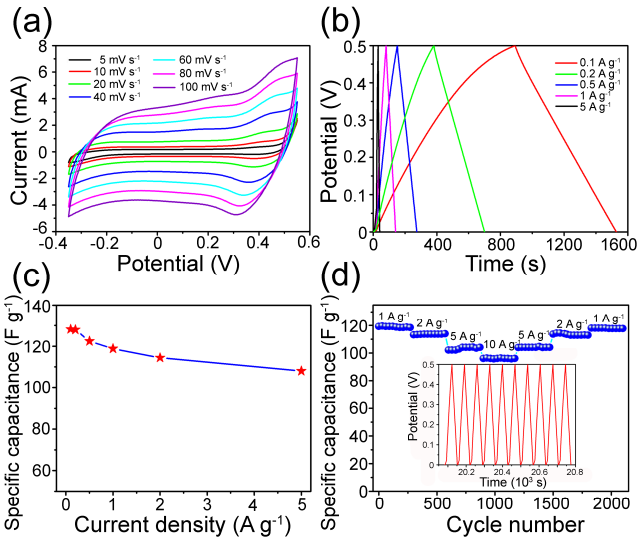

Fig. 5 (a) CV curves at different scan rates. (b) Galvanostatic charge-discharge curves at different current densities. (c) Specific capacitance of the $MnCo_2O_{4.5}$ electrode as a function of the current density. (d) CD cycling stability of the $MnCo_2O_{4.5}$ electrode at progressively varied current densities, and the inset shows charge-discharge curves at a current density of 1 A g^{-1}.

To explore the potential power applications of the porous urchin-like $MnCo_2O_{4.5}$ hierarchical architectures, the sample was fabricated into the supercapacitor electrode and capacitive performances were evaluated with cycle voltammogram (CV) and galvanostatic charge-discharge (CD) measurements. Fig. 5a shows the CV curves of the $MnCo_2O_{4.5}$ electrode at different scan rates measured between -0.35 and 0.55 V. It can be clearly observed that all the curves show approximate rectangular shape and symmetric CV curves, indicating that the Faraday redox reactions are electrochemically reversible and present an ideal supercapacitor behavior. A specific capacitance of 151.2 F g^{-1} is obtained at scan rate of 5 mV s^{-1} (other values are shown in Table 1, in ESI†). Notably, as the scan rate increasing from 5 to 100

mV s^{-1}, the shape of the CV curves basically remains unchanged except for the small shift of the peak position, indicating the excellent electrochemical reversibility and outstanding high-rate performance. In addition, the graphite paper substrate may influence the final CV curves with a small capacitance contribution, so we compared it with the $MnCo_2O_{4.5}$ electrode (Fig. S5, in ESI†) and found that its effect to the results is negligible. Galvanostatic CD curves for the $MnCo_2O_{4.5}$ electrode measured between 0 and 0.5 V at different current densities are shown in Fig. 5b. A high symmetric nature is observed in all the charging-discharging curves, indicating an ideal electrochemical capacitive characteristic and superior reversible redox reaction in the whole potential region. The specific capacitances of the materials evaluated from the discharge curves were 129.2, 127.9, 122.4, 118.8 and 108 F g^{-1} at current densities of 0.1, 0.2, 0.5, 1 and 5 A g^{-1}, respectively.

Rate capability is an important factor for the use of supercapacitors in power applications. A good electrochemical energy storage device is required to keep a high specific capacitance retention at high charge-discharge rate. The variation of the specific capacitance of $MnCo_2O_{4.5}$ electrode with an increase in current density is shown in Fig. 5c. As can be seen, the $MnCo_2O_{4.5}$ electrode preserved 83.6% of its specific capacitance (from 129.2 to 108 F g^{-1}) as the current density increases from 0.1 to 5 A g^{-1} (50 times increase). The remarkable rate capability can be attributed to the unique porous structure of the materials. The highly porous framework allows the facile penetration of electrolyte that promotes the surface and near surface redox reactions, and guarantees a relatively highly electrolytic accessible area. Thus a high specific capacitance retention can be obtained even at high rates.[13,26] Moreover, the rate capability of the porous $MnCo_2O_{4.5}$ hierarchical structures is considered to be very outstanding compared with many reported MTMO nanostructurs for supercapacitors, for instance, $NiCo_2O_4$ nanorods and nanosheets (48.8% and 51.9% retention with 20 times increase),[12] porous $NiCo_2O_4$ nanowires (78.6% retention with 40 times increase),[13] $CoFe_2O_4$ nanorings (81.3% retention with 20 times increase),[14] $NiMn_2O_4$ nanorings (11.1% retention with 8 times increase).[15] In addition, electrochemical impedance spectroscopy (EIS) was also employed to characterize the composite electrodes (Fig. S6, in ESI†), the equivalent series resistance (ESR) value of the porous $MnCo_2O_{4.5}$ hierarchical was only 1.3 Ω, which was much lower than the precursor (7.4 Ω), indicating the improved charge transport properties of the porous electrodes.

The cycle performance is of great importance for supercapacitors. The electrochemical stability of $MnCo_2O_{4.5}$ electrode at progressively increased current density was recorded and shown in Fig. 5d. As can be seen, during the first 300 cycles with a charge-discharge density of 1 A g^{-1}, the electrode keeps a nearly stable specific capacitance of 118.8 F g^{-1}. Even suffering from sudden change of the current densities, the electrode exhibits stable capacitance at each current density. When the current turns back to 1 A g^{-1} after 2100 cycles, a fully recovered specific capacitance of 118 F g^{-1} is observed after the finial 300 cycles, which confirms the $MnCo_2O_{4.5}$ electrode has outstanding rate capability, the insert image shows the last 10 charge-discharge cycles of the last stage, after charge-discharge cycling for 20775 s, the charge curves are still very symmetric to their corresponding discharge counterparts, showing the excellent cycling stability of the $MnCo_2O_{4.5}$ electrode. These results highlight the capability of the MTMOs material electrode to meet the requirements of both good rate capability and long cycle lifetime, which are important merits for practical energy storage devices.

4. Conclusions

In summary, we have demonstrated a facile synthesis of porous urchin-like $MnCo_2O_{4.5}$ hierarchical structures, which exhibited a specific capacitance of 151.2 F g^{-1} at scan rate of 5 mV s^{-1}. More importantly, this unique electrode demonstrated an outstanding rate capability with 83.6% retention even at the current density increasing to 50 times (0.1 to 5 A g^{-1}), and showed excellent long-term cycle stability that it nearly had no decrease after 2100 cycles at progressively varied current densities. Such intriguing capacitive behaviors are mainly attributed to the unique porous and robust hierarchical architectures. Although the specific capacitance is not high, it is reckoned that the present $MnCo_2O_{4.5}$ hierarchical structures can serve as a promising electrode material for high-rate supercapacitors in some special applications which is not work with high capacitance.

Acknowledgements

This work was financially supported by the National Natural Science Foundation of China (Grant Nos. 21171035 and 51302035), the Key Grant Project of Chinese Ministry of Education (Grant No. 313015), the PhD Programs Foundation of the Ministry of Education of China (Grant Nos. 20110075110008 and 20130075120001), the National 863 Program of China (Grant No. 2013AA031903), the Science and Technology Commission of Shanghai Municipality (Grant No. 13ZR1451200), the Fundamental Research Funds for the Central Universities, the Shanghai Leading Academic Discipline Project (Grant No. B603), and the Program of Introducing Talents of Discipline to Universities (No. 111-2-04).

Notes and references

[a] *State Key Laboratory for Modification of Chemical Fibers and Polymer Materials, College of Materials Science and Engineering, Donghua University, Shanghai 201620, China. Fax: +86-21-6779-2947; Tel: +86-21-6779-2947;E-mail: rjzou@dhu.edu.cn; hu.junqing@dhu.edu.cn;*
[b] *School of material engineering, Shanghai university of engineering science, Shanghai 201620, China*

† Electronic Supplementary Information (ESI) available: [Experimental process, Supplementary Fig.s and Specific capacitance calculation]. See DOI: 10.1039/b000000x/

1 D D. R. Rolison, J. W. Long, J. C. Lytle, A. E. Fischer, C. P. Rhodes, T. M. McEvoy, M. E. Bourg, A. M. Lubers, *Chem. Soc. Rev.*, 2009, **38**, 226.
2 J. R. Miller, P. Simon, *Science*, 2008, **321**, 651.
3 P. Simon, Y. Gogotsi, *Nat. Mater.*, 2008, **7**, 845.
4 G. Wang , L. Zhang, J. Zhang, *Chem. Soc. Rev.*, 2012, **41**, 797.
5 W. Y. Li, Q. Liu, Y. G. Sun, J. Q. Sun, R. J. Zou, G. Li, X. H. Hu, G. S. Song, G. X. Ma, J. M. Yang, Z. G. Chen, J. Q. Hu, *J. Mater. Chem.*, 2012, **22**, 14864.
6 R. B. Rakhi, W. Chen, D. Cha, H. N. Alshareef, *Nano Lett.*, 2012, **12**, 2559.

7 Q. Lu, M. W. Lattanzi, Y. Chen, X. Kou, W. Li, X. Fan, K. M. Unruh, J. G. Chen, J. Q. Xiao, *Angew. Chem. Int. Ed.*, 2011, **50**, 6847.

8 J. Benson, S. Boukhalfa, A. Magasinski, A. Kvit, G. Yushin, *ACS Nano*, 2012, **6**, 118.

9 G. Zhang, L. Yu, H. B. Wu, H. E. Hoster, X. W. Lou, *Adv. Mater.*, 2012, **24**, 4609;

10 T. Y. Wei, C. H. Chen, H. C. Chien, S. Y. Lu, C. C. Hu, *Adv. Mater.*, 2010, **22**, 347.

11 L. Zhou, D. Zhao, X. W. Lou, *Adv. Mater.*, 2012, **24**, 745.

12 G. Zhang, X. W. Lou, *Sci. Rep.*, 2013, **3**, 1470.

13 H. Jiang, J. Ma, C. Z. Li, *Chem. Commun.*, 2012, **48**, 4465.

14 D. H. Deng, H. Pang, J. M. Du, J. W. Deng, S. J. Li, J. Chen, J. S. Zhang, *Cryst. Res. Technol.*, 2012, **47**, 1032.

15 M. Zhang, S. H. Guo, G. N. Zhang, Z. P. Hao, L. P. Kang, Z. H, Liu, *Electrochim. Acta*, 2013, **87**, 546.

16 J. B. Fei, Y. Cui, X. H. Yan, W. Qi, Y. Yang, K. W. Wang, Q. He, J. B. Li, *Adv. Mater.*, 2008, **20**, 452.

17 G. B. Sun, B. X. Dong, M. H. Cao, B. Q. Wei, C. W. Hu, *Chem. Mater.*, 2011, **23**, 1587.

18 B. Wang, J. S. Chen, H. B. Wu, Z. Y. Wang, X. W. Lou, *J. Am. Chem. Soc.*, 2011, **133**, 17146.

19 H. B. Li, M. H. Yu, F. X. Wang, P. Liu, Y. Liang, J. Xiao, C. X. Wang, Y. X. Tong, G. W. Yang, *Nat. Commun.*, 2013, **4**, 1894.

20 X. F. Wang, B. Liu, Q. F. Wang, W. F. Song, X. J. Hou, D. Chen, Y. B. Cheng, G. Z. Shen, *Adv. Mater.*, 2013, **25**, 1479.

21 Y. H. Xiao, S. J. Liu, F. Li, A. Q. Zhang, J. H. Zhao, S. M. Fang, D. Z. Jia, *Adv. Funct. Mater.*, 2012, **22**, 4052.

22 M. K. Song, S. Cheng, H. Chen, W. Qin, K. W. Nam, S. Xu, X. Q. Yang, A. Bongiorno, J. Lee, J. Bai, T. A. Tyson, J. Cho, M. L. Liu, *Nano Lett.*, 2012, **12**, 3483.

23 S. H. Yu, H. Colfen, M. J. Antoniietti, *J. Phys. Chem. B*, 2003, **107**, 7396.

24 Q. F. Wang, B. Liu, X. F. Wang, S. H. Ran, L. M. Wang, D. Chen, G. Z. Shen, *J. Mater. Chem.*, 2012, **22**, 21647.

25 Y. G. Sun, R. J. Zou, W. Y. Li, Q. W. Tian, J. H. Wu, Z. G. Chen, J. Q. Hu, *CrystEngComm*, 2011, **13**, 6107.

26 C. Yuan, J. Li, L. Hou, X. Zhang, L. Shen, X. W. Lou, *Adv. Funct. Mater.*, 2012, **22**, 4592.

The table of contents entry

A supercapacitor electrode of porous urchin-like manganese cobalt oxide ($MnCo_2O_{4.5}$) hierarchical architectures, which were synthesized via a facile hydrothermal route followed a thermal annealing process, demonstrated an outstanding rate capability and excellent cycling stability, which could be considered as a perspective mixed transition metal oxides material for high-rate supercapacitors.